# Mobility and trapping of hydrogen in high-strength steel

Flavien Vucko, Asdin Aoufi, Cédric Bosch, David Delafosse

# Mobility and trapping of hydrogen in high-strength steel

*Vucko Flavien, Aoufi Asdin, Bosch Cédric, Delafosse David,*
*Ecole Nationale Supérieure des Mines, SMS-EMSE, CNRS: UMR 5307, LGF, 158 cours Fauriel, 42023 Saint-Etienne, France*

## Summary

Electrochemical permeation and thermo-desorption tests are performed to evaluate hydrogen mobility in high strength steel. Experimental parameters are used in a Krom like phenomenological diffusion model. This model is developed to simulate hydrogen diffusion and trapping in processing zones of specimens subjected to fatigue loadings.

## 1 Introduction

Hydrogen is known to be very detrimental to the mechanical properties of steels [1,2]. The sensitivity to hydrogen embrittlement increases with the strength of the material [3]. Many premature failures of high-strength steels in industrial applications are due to the presence of hydrogen.
Hydrogen embrittlement mechanisms are closely linked to the mobility and the segregation of hydrogen in the material. Microstructural defects, as trapping sites, are particularly involved in these mechanisms as reservoirs for diffusible hydrogen (reversible traps) or as promoters of its mobility (mobile traps like mobile dislocations [4]). A phenomenological model was proposed by Krom [5] to simulate hydrogen diffusion and trapping. The model is well established for monotonic mechanical loading, but needs further development in cyclic strain conditions. Electrochemical permeation (EP) and thermal desorption spectroscopy (TDS) are two interesting techniques to study hydrogen mobility and trapping [6–9]. The first one informs us about the diffusion coefficient and the content of trapped hydrogen, and the second one gives access to the trapping energy. These methods are applied to a quenched-tempered martensitic steel S690QL in order to develop a model of diffusion/trapping during fatigue loading. Additional analyses are used to establish evolution laws for trapping sites.
This paper is divided into three parts. The first part is related to the material and experimental procedures. The second part focuses on the diffusion model laws constructed from experimental data. Finite element simulations are described in the third part.

## 2 Material and experimental procedures

### 2.1 Material

The material of the study is a high strength steel S690QL (EN 10137-2). It exhibits a tempered martensitic microstructure consisting of laths of about 200 nm wide. Laths are gathered in blocks and packets which are included in prior austenite grain with a size ranging from 10 to 20 µm. The steel chemical composition is given in table 1. The tempering duration and temperature were two hours at 550°C after austenitization at 920°C. No retained austenite was revealed by X-ray analysis. This

kind of microstructure exhibits many heterogeneities which are hydrogen trapping sites (see figure 1) with characteristic energies.

Table 1: Chemical composition of steel S690QL (weight %)

| Elements | C | Si | Mn | Mo | Nb | Ni | Ti | S |
|---|---|---|---|---|---|---|---|---|
| wt.% | 0.16 | 0.33 | 1.22 | 0.25 | ≤0.10 | 0.11 | ≤0.05 | ≤0.001 |
| Elements | P | V | Zr | N | B | Cr | Cu | Fe |
| wt.% | ≤0.02 | ≤0.1 | ≤0.1 | ≤0.015 | ≤0.005 | 0.29 | ≤0.1 | Bal. |

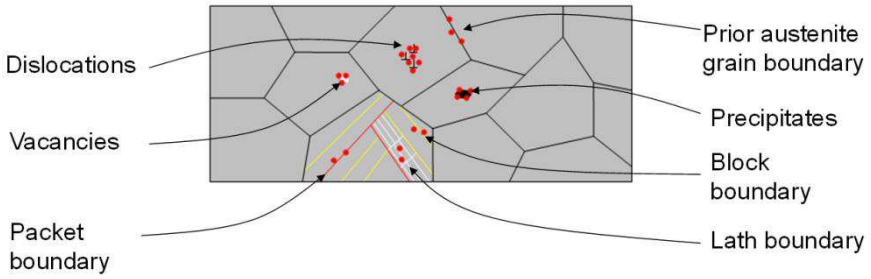


**Figure 1:** Trapping sites in quench-tempered microstructure

## 2.1 Electrochemical permeation

EP tests are performed in Devanathan and Stachurski [8] link device consisting of a charging cell and an oxidation (or detection) cell. Both cells are filled with 0.1 M sodium chloride solution deoxygenated by nitrogen. The steel sample is cylindrical membrane with a thickness of 0.6 mm and a diameter of 40 mm. Mechanical polishing with SiC paper is performed on both faces up to grade 4000. A thin palladium coating (230 nm) is deposited on detection side by an electrochemical process. The membrane is mounted in a holder which reduces the contact surface to a circular area of 1 cm² on both faces. Platinum counter electrode and saturated calomel electrode are used in each cell and the steel sample is the common working electrode. A floating ground galvanostat is plugged to the charging cell and a potentiostat to the detection side. The detection side is continuously polarized at -100mV/ECS. The charging side of the sample is subjected to a cathodic current (-5 to -30 mA/cm²). The recorded anodic current on the detection side is the permeation rate of hydrogen through the membrane.

## 2.2 Thermal desorption spectrometry

TDS experiments are widely used to study hydrogen trapping in metals [7,10,11]. This technique consists in heating a metal sample at a determined rate in vacuum (<$10^{-5}$ mbar) and recording the amount of gas desorbed with a mass spectrometer. Hydrogen pre-charging is performed by cathodic polarization in a 30 $g.L^{-1}$ NaCl solution at $E_c$=-1200 mV/SCE for 64 hours. The solution was de-aerated and buffered at pH 4.5 by bubbling a gas mixture of $N_2$-7%$CO_2$. Cylindrical samples are machined from tensile or fatigue specimens.

As demonstrated in literature [10,12], analytical models based on Kissinger equilibrium [13] are quite accurate for low hydrogen concentration and low trapping site occupancy, i.e. low trapping energy. Choo and al. [7] demonstrated that detrapping energy $E_{TL}$ can be related to the temperature at the maximum desorption peak $T_p$, i.e. the maximum hydrogen desorption rate, with the equation (Eq.1):

$$\partial \ln\left(a/T_p^2\right)/\partial\left(1/T_p\right) = \frac{-E_{TL}}{R} \qquad \text{Eq.1}$$

where $a$ is the heating rate of the thermal desorption test.
As a consequence, trapping energies are determined by testing samples at different heating rates. But spectrum deconvolution is necessary to separate each peak.

### 2.3 Additional analyses

Plastic strain controlled low cycle fatigue tests are analysed using Handfield and Dickson's method [14]. The internal stress X, the thermal effective stress Σ* and the athermal effective stress $\Sigma_\mu$ are determined for each hysteresis cycle. These stresses are related to microstructural defects evolution.
Dislocation density is investigated by X-Ray line profile analysis [15]. Indeed, peak broadening is related to dislocation density. The momentum method [16–18] is applied to determine the dislocation density evolution during cyclic loading. Data are recorded using Panalytical MRD device with Co $K_\alpha$ radiation (1.790 Å) and optics equipped with a slit of 1/8°.
Microstructural investigation by transmission electron microscopy (TEM) on fatigue specimens is performed using a PHILIPS FEI CM 200 device operating at 200 kV. Thin samples with a diameter of 3 mm and a thickness of 100 µm are machined from fatigue specimens by saw-wire cutting. Final thickness (< 200 nm) is obtained by electropolishing in 10%-perchloric acid with ethanol at 15 V for about 40 s.

## 3 Diffusion model

The diffusion equation of the model is given by Krom [5]:

$$\left(1+\frac{C_T}{C_L}\left(1-\frac{C_T}{N_T}\right)\right)\frac{\partial C_L}{\partial t}=\nabla.\left(D_L\nabla C_L\right)-\nabla.\left(\frac{D_L V_H}{RT}C_L\nabla(\sigma_H)\right)-\theta_T\frac{\partial N_T}{\partial \varepsilon_p}\dot{\varepsilon}_p \qquad \text{Eq.2}$$

For cyclic loading, the number of traps $N_T$ is a function of both the plastic strain $\varepsilon_p$ and the cumulative plastic strain p. Evolution laws are determined for each kind of trap.
Five different traps are detected by TDS analyses. Their trapping energies are reported in table 2. Total hydrogen concentration is also determined by katharometry and its concentration in each trap is given by TDS peak area ratios. With the assumption that the steel lattice is filled with hydrogen in our charging conditions, the number of traps can be directly extracted from this data.

Table 2: Trapping sites energies from TDS

| TDS peak | 1 | 2 | 3 | 4 | 5 |
|---|---|---|---|---|---|
| Energy (eV) | 0.14+/-0.05 | 0.11+/-0.02 | 0.23+/-0.05 | 0.70+/-0.10 | 0.64+/-0.09 |

Traps are attributed to possible microstructural defects. Some of them are strongly influenced by plastic strain (peaks 2 and 3) and probably related to dislocation density and cells formation respectively. The model is mainly focused on these defects.
Dislocation density is determined by X-Ray diffraction and cell walls developed during fatigue loading are measured by both TEM and X-Ray diffraction. Their evolutions are modeled using equations similar to those used by Kumnick and Johnson [19] to fit experimental data:

$$log(N_{T1}) = A - B.e^{-C.|\varepsilon_p|} + D.e^{-E.p} \quad \text{Eq.3}$$

$$log(N_{T2}) = A' - B'.e^{-C'.p} \quad \text{Eq.4}$$

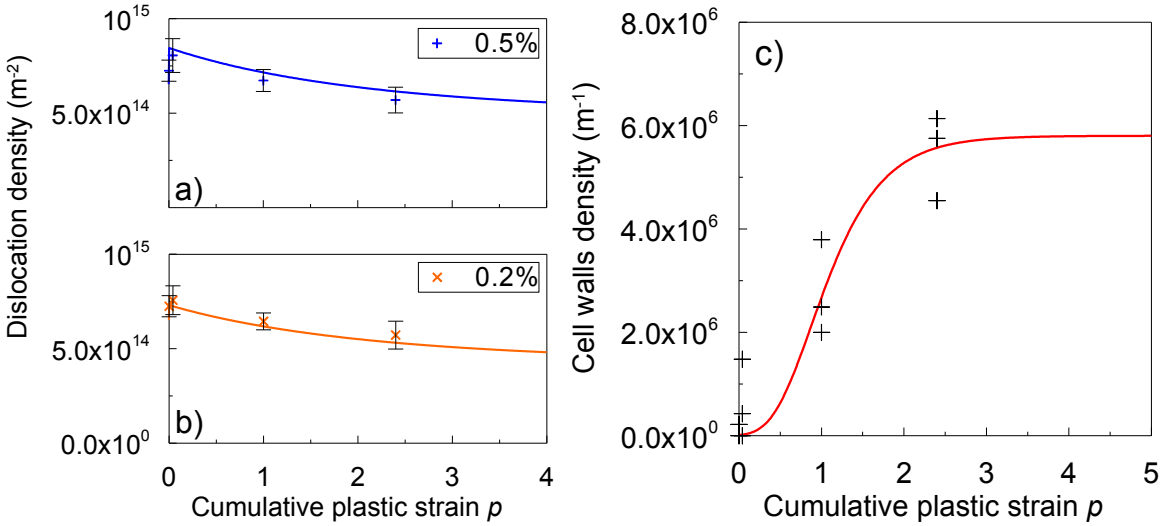


**Figure 2:** Evolution of the dislocation density from equation 3 for low cycle fatigue tests at half strain amplitude of a) 0.5% and b) 0.2%. c) Evolution of the cell walls density from equation 4.

As shown in figure 2, the global dislocation density decreases with plastic strain accumulation, whereas cell walls density increases until saturation state.

# 4 Finite elements simulations

## 4.1 Two traps model

One-dimensional model is developed to compute diffusion and trapping of hydrogen with two different trapping energies. The geometry is constructed to simulate electrochemical permeation test with a main part ($\Omega_L$=[0,$e_L$]) of $e_L$=600 µm and a thin layer, called "coating", ($\Omega_c$=[$e_L$,$e_L$+$e_c$]) of $e_c$=0.23 µm.

Hydrogen diffusion is nonlinear in the main part as proposed by Sofronis [20]. Equation is presented below.

$$\forall x \in \Omega_L: \quad \left(1 + \sum_i \frac{C_{T_i}(x,t)}{C_L(x,t)}\left(1 - \frac{C_{T_i}(x,t)}{N_{T_i}}\right)\right)\frac{\partial C_L}{\partial t}(x,t) = \nabla.\left(D_L \nabla C_L(x,t)\right) \quad \text{Eq.5}$$

$C_T$ and $C_L$ are respectively the trapped and lattice hydrogen concentration. $N_T$ is the number of trapping sites. The apparent lattice diffusion coefficient $D_{eff}$ is calculated from Eq.6:

$$D_{eff}\left(C_L(x,t), C_{T_1}(x,t), C_{T_2}(x,t)\right) = \frac{D_L}{1+\sum_{i=1}^{2}\frac{C_{T_i}(x,t)}{C_L(x,t)}\left(1-\frac{C_{T_i}(x,t)}{N_{T_i}}\right)} \quad \text{Eq.6}$$

$D_L$ is the true lattice diffusion coefficient without any trapping.

The diffusion coefficient is constant in the coating and no trapping occurs. Diffusion respects the 2nd Fick's law.

Different boundary conditions are tested at the entrance and at the exit sides to match experimental data. At the interface x=$e_L$, flux continuity with or without concentration continuity is tested.

Concentration and diffusion coefficient profiles are presented in figure 3. These simulations are computed with two trapping energies 0.11 and 0.23 eV. As shown in figure 3b, the diffusion coefficient is weakly affected by trapped hydrogen, and

concentration profiles are quite similar, except the maximum value. These profiles are strongly changed for higher trapping energies.

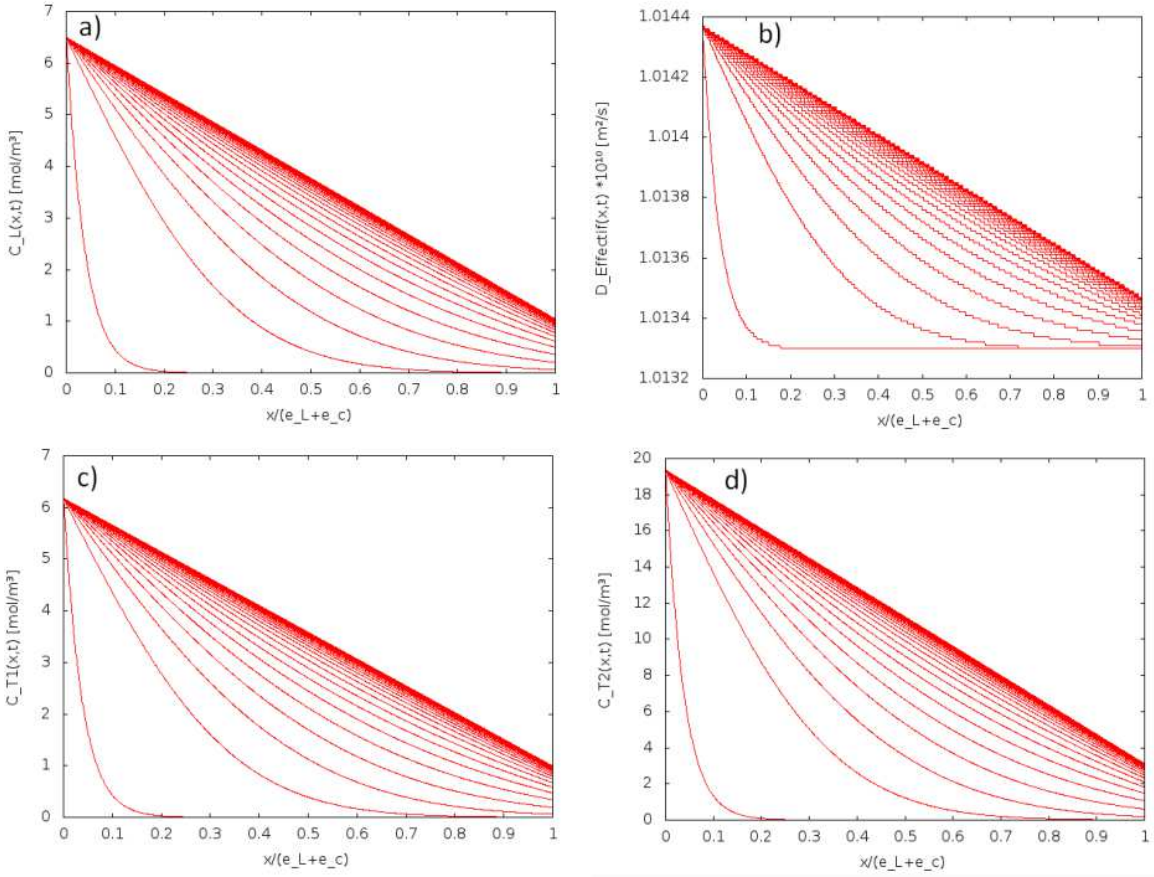


**Figure 3:** a) Concentration profiles of lattice hydrogen. b) Evolution of the apparent diffusion coefficient in the steel. c) and d) Concentration profiles of trapped hydrogen.

## 4.2 Mechanical loading

Hydrogen diffusion is affected by the elasticity and the plasticity. A two-dimensional model is currently developed to take into account mechanics in the model. The geometry is representative of hydrogen assisted cracking test specimens, with micro-notch as presented in figure 4. Hydrogen concentration at the notch-tip is expected during cyclic loading.

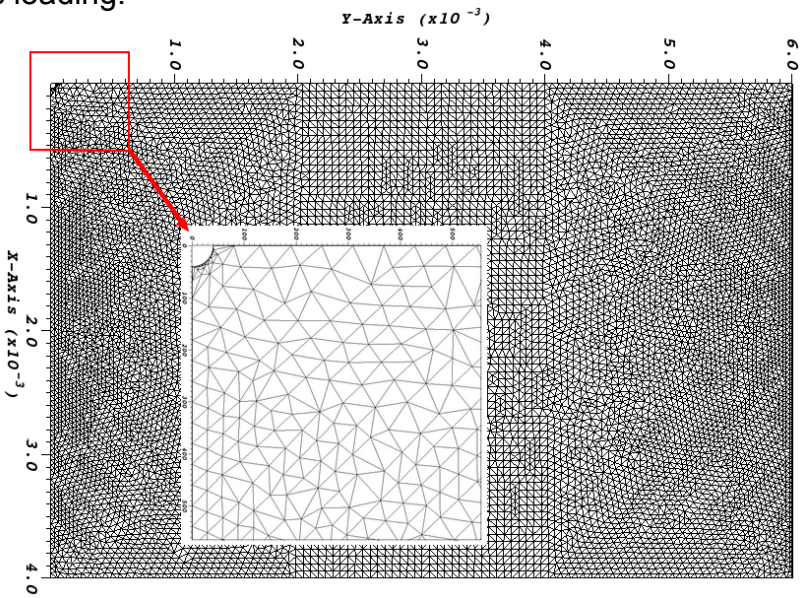


**Figure 4:** Geometry of notched specimens

# 5 Conclusion

Hydrogen mobility and trapping in high-strength steel is studied by electrochemical permeation and thermal desorption spectrometry. Five different trapping energies are detected and related to microstructural defects. An analytical relationship between plastic strain and trap density is used for the mechanical/diffusion coupling. The diffusion coefficient is weakly affected by trapped hydrogen in low trapping energy sites.
Finite element analysis is under investigation to fully simulate hydrogen assisted cracking tests.

# 6 References


[1] G. Sandoz, Metallurgical Transactions 3 (1972) 1169.
[2] D. Hardie, E.A. Charles, A.H. Lopez, Corrosion Science 48 (2006) 4378.
[3] N.E. Nanninga, Y.S. Levy, E.S. Drexler, R.T. Condon, A.E. Stevenson, A.J. Slifka, Corrosion Science 59 (2012) 1.
[4] J.A. Donovan, Metallurgical Transactions A 7 (1976) 1677.
[5] A. Krom, R. Koers, A. Bakker, Journal of the Mechanics and Physics of Solids (1999) 860.
[6] P.A. Redhead, Vacuum 12 (1962) 203.
[7] W. Choo, J. Lee, Metallurgical and Materials Transactions A 13 (1982) 135.
[8] M.A. V. Devanathan, Z. Stachurski, Proceedings of the Royal Society A: Mathematical, Physical and Engineering Sciences 270 (1962) 90.
[9] T. Zakroczymski, Journal of Electroanalytical Chemistry 475 (1999) 82.
[10] A. Turnbull, R. Hutchings, D. Ferriss, Materials Science and Engineering: A 238 (1997) 317.
[11] S. Frappart, A. Oudriss, X. Feaugas, J. Creus, J. Bouhattate, F. Thébault, L. Delattre, H. Marchebois, Scripta Materialia 65 (2011) 859.
[12] L. Cheng, M. Enomoto, F.-G. Wei, ISIJ International 53 (2013) 250.
[13] H.E. Kissinger, Analytical Chemistry 29 (1957) 1702.
[14] J.I. Dickson, J. Boutin, L. Handfield, Materials Science and Engineering 64 (1984) L7.
[15] P. Gay, P. Hirsch, A. Kelly, Acta Metallurgica 1 (1953) 315.
[16] A. Borbély, J.H. Driver, T. Ungár, Acta Materialia 48 (2000) 2005.
[17] A. Borbély, A. Révész, I. Groma, Zeitschrift Für Kristallographie Supplements 2006 (2006) 87.
[18] A. Borbély, T. Ungár, Comptes Rendus Physique 13 (2012) 293.
[19] A.J. Kumnick, H.H. Johnson, Acta Metallurgica 28 (1980) 33.
[20] P. Sofronis, R.M. McMeeking, Journal of the Mechanics and Physics of Solids 37 (1989) 317.